HHS Public Access

Author manuscript

J Comp Neurol. Author manuscript; available in PMC 2019 October 15.

Published in final edited form as:

J Comp Neurol. 2018 October 15; 526(15): 2373–2387. doi:10.1002/cne.24491.

Extensive Somatosensory and Motor Corticospinal Sprouting Occurs Following a Central Dorsal Column Lesion in Monkeys

Karen M. Fisher, **Alayna Lilak**, **Joseph Garner**, and **Corinna Darian-Smith**

Department of Comparative Medicine, Stanford University School of Medicine, 300 Pasteur Drive, Stanford, CA94305-5342

Abstract

The corticospinal tract (CST) forms the major descending pathway mediating voluntary hand movements in primates, and originates from nine cortical subdivisions in the macaque. While the terminals of spared motor CST axons are known to sprout locally within the cord in response to spinal injury, little is known about the response of the other CST subcomponents. We previously reported, that following a cervical dorsal root lesion (DRL), the primary somatosensory (S1) CST terminal projection retracts to 60% of its original terminal domain, while the primary motor (M1) projection remains robust (Darian-Smith et al., J. Neurosci., 2013). In contrast, when a dorsal column lesion (DCL) is added to the DRL, the S1 CST, in addition to the M1 CST, extends its terminal projections bilaterally and caudally, well beyond normal range (Darian-Smith et al., J. Neurosci., 2014). Are these dramatic responses linked entirely to the inclusion of a CNS injury (i.e. DCL), or do the two components summate or interact? We addressed this directly, by comparing data from monkeys that received a unilateral DCL alone, with those that received either a DRL or a combined DRL/DCL. Approximately four months post-lesion, the S1 hand region was mapped electrophysiologically, and anterograde tracers were injected bilaterally into the region deprived of normal input, to assess spinal terminal labeling. Using multifactorial analyses, we show that following a DCL alone (i.e. cuneate fasciculus), the S1 and M1 CSTs also sprout significantly and bilaterally beyond normal range, with a termination pattern suggesting some interaction between the peripheral and central lesions.

Graphical Abstract

Somatosensory corticospinal (S1 CST) terminal fields were mapped in the spinal cord of monkeys after dorsal root (DRL), dorsal column (DCL), or combined lesions (DRL/DCL). Sectioning dorsal roots reduced input to the cord, but lesions involving the central dorsal column (I.e. DCLs or combined DRL/DCLs), induced considerable bilateral sprouting.

Corresponding and submitting author: Corinna Darian-Smith, Tel.: 650 736 0969, Fax: 650 498 5085, cdarian@stanford.edu.

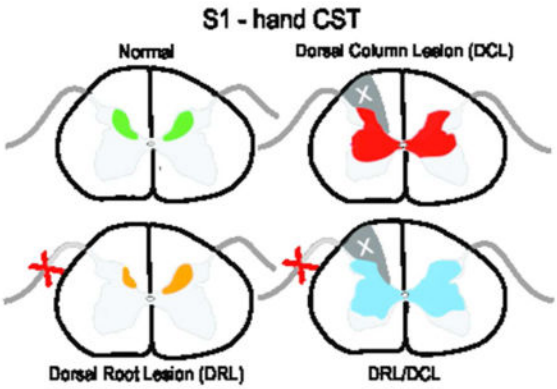

Keywords

spinal cord injury; corticospinal tract; primary afferent lesion; somatosensory; motor; dorsal column; nonhuman primate; functional recovery; RRID: AB_2536190; RRID: AB_2313606

Introduction

The corticospinal tract (CST; see Table 1 for all acronyms) is the primary descending pathway controlling hand dexterity in primate species, and injury to this pathway is well known to impact fine volitional movements of the hands (Lawrence & Kuypers, 1968). Not surprisingly, injury to the ascending pathways, which provide ongoing sensory feedback that informs motor output, can also dramatically impair hand and limb function (Darian-Smith & Brown, 2000; Qi, Gharbawie, Wynne, & Kaas, 2013), including the quality of movements of the hand (Darian-Smith & Ciferri, 2005; Glendinning, Cooper, Vierck, & Leonard, 1992; Leonard, Glendinning, Wilfong, Cooper, & Vierck, 1992; Murphy et al., 2003; Sainburg, Poizner, & Ghez, 1993). The CST has multiple cortical origins in primates. Projections originating in the primary motor cortex (M1 = Brodmann Area 4), primary somatosensory cortex (S1= Areas 3a, 3b, 1, and 2), and the supplementary motor area (SMA), together contribute the largest inputs to the cervical cord, but ~25% of the CST originates from still other cortical sites (Dum & Strick, 1991; Galea & Darian-Smith, 1994). Though we still know relatively little about the role of the different sensorimotor CST pathways in the recovery process following spinal cord injury (SCI), understanding their respective contributions is fundamental to designing and targeting informed therapeutic strategies for optimizing recovery.

In rats, compensatory sprouting from spared fibers in the motor CST has been shown to coincide with the recovery of forelimb function following CST injury (Carmel, Kimura, Berrol, & Martin, 2013; Jiang, Zaaimi, & Martin, 2016; Lindau et al., 2014; Weidner, Ner, Salimi, & Tuszynski, 2001), though the motor and somatosensory CST subcomponents have not been clearly differentiated. In primates, the M1 CST has similarly been linked to the recovery of hand function after SCI (Friedli et al., 2015; Galea & Darian-Smith, 1997a, 1997b; Rosenzweig et al., 2010), but until recently, nothing was known specifically about the primary somatosensory CSTs contribution following SCI. We now know that following a

peripheral DRL (Darian-Smith, Lilak, & Alarcon, 2013; Darian-Smith, Lilak, Garner, & Irvine, 2014), the M1 CST remains robust but does not sprout significantly beyond its normal terminal territory, while the S1 (Areas 3b/1) CST retracts to 60% of its normal terminal territory. Additionally, when the cuneate fasciculus of the dorsal column (DCL) is also cut to create a combined DRL/DCL, to better simulate a clinical injury, both the M1 and S1 CSTs sprout dramatically in the ensuing months (Darian-Smith et al., 2014). The CST terminal sprouting from Areas 3b/1 has been shown to be particularly striking (see Figure 4 summarizing earlier findings), given the 40% retraction of this pathway following the DRL alone.

These findings raised the following questions, which we address in the present study: *Why was there a retraction of the Areas 3b/1 CST and little evidence of M1 CST terminal sprouting following a peripheral deafferentation, but extensive bilateral terminal sprouting when a small cuneate fasciculus lesion was added to the injury? Was the M1 and S1 CST axonal sprouting observed following the combined lesion a direct result of the central nervous system being injured, or was it the result of an interaction or summation of the two lesions (one peripheral and one central)*? To address this gap in our understanding, we selectively lesioned the cuneate fasciculus of the dorsal column on its own. This created a purely central (partial primary afferent) injury. We then compared CST responses of this central lesion on its own, with data from monkeys used in earlier investigations (Darian-Smith et al., 2013; Darian-Smith et al., 2014), where animals had received either a peripheral (DRL), or combined DRL/DCL.

The DRLs (i.e. dorsal rhizotomies) alone removed all detectable primary afferent input (i.e. cutaneous, proprioceptive, spinothalamic, spinoreticular, etc), from the first 3 digits of one hand. The DCL, in contrast, which only involved the lateral cuneate fasciculus in our animals (see Figures 1, 2), caused a less debilitating partial deafferentation, since it removed the major mechanoreceptor and proprioceptor inputs from the hand (and part of the arm), but left spinothalamic, spinoreticular, and other central pathways intact. Though dorsal column lesions are partial deafferentations, they are known to induce large scale reorganisation upstream in the cuneate nucleus (Kambi et al., 2014), thalamus (Jain, Qi, Collins, & Kaas, 2008), and cortex (Qi, Chen, & Kaas, 2011). Since our lesion models are precise and repeatable our experimental approach allows us to dissect out specific pathway responses and involvement in small numbers of animals; something not possible otherwise.

Our findings indicate that even a small central DCL is critical for extensive CST terminal sprouting to occur during the post-lesion months, and that combined peripheral and central injuries result in termination patterns that reflect a complex interaction between the peripheral and central lesion components. Understanding such interactions provides insight into the mechanisms that drive recovery in more complex clinical injuries, where both peripheral and central elements are typically involved.

Materials and Methods

Data were combined from 10 monkeys in this study (2 DCL, 6 DRL, and 2 combined DRL/DCL; see Table 2). Some of the data from 8 of these monkeys were used in earlier studies

(Darian-Smith et al., 2013, 2014). Additional data were obtained however from all monkeys used in previous reports, to ensure that data sets were comparable across animals. Importantly, the experimental methods used throughout these experiments were always the same unless specifically indicated (e.g. the different lesion types).

All monkeys were healthy young adult male macaques (*Macaca fascicularis*; 2.0–3.8kg, s.d. ±0.57, 3.5–4.5 years old). Monkeys were colony bred (Charles River), and housed individually at the Stanford Research Animal Facility, with access to four unit cages (64×60×77cm, depth x width x height per each unit) in a room with other monkeys and a 12 hour light/dark cycle. Animals had freely available water and primate diet, supplemented daily with fresh fruit, vegetables, and a variety of nuts, cereal, and novel foods. They also had daily enrichment in the form of behavioral training, primate toys, videos and music.

All animal procedures were carried out in accordance with National Institutes of Health guidelines and ethical approval was granted by the Stanford University Institutional Animal Care and Use Committee.

All monkeys underwent an identical sequence of procedures, the details of which are provided below. These included an initial laminectomy, during which recordings were made from dorsal rootlets and lesions created. Approximately 5 months later, they underwent a bilateral craniotomy, during which the S1 cortex was mapped electrophysiologically, and tracer injections were made into S1 and motor cortex. Monkeys then survived for an additional 6–7 weeks, at which point they were perfused for tissue processing. Details and timelines are provided for each animal in Table 2.

Surgical procedures

For all surgical procedures, anesthesia was induced with ketamine hydrochloride (10mg/kg), and surgery performed using gaseous anesthesia maintained with isofluorane (1–2% in/1% O_2), using a standard open circuit anesthetic machine. Atropine sulphate (0.05mg/kg), buprenorphine (0.01mg/kg) and the antibiotic cefazolin (20mg/kg) were administered initially as loading doses, and saline was infused (i.v.) throughout surgery to maintain fluid balance.

Monkeys were kept warm using a thermostatically controlled heating pad and an air blanket (Bair Hugger). Physiological signs were monitored throughout surgery to ensure a deep, stable anesthesia (i.e. blood pressure, heart rate, pulse oximetry, capnography, core temperature).

Spinal cord lesions were unilateral (laterality is indicated in Table 2), and the lesion was made on the side of the dominant hand to encourage its use following injury. Hand preference was assessed where possible with behavioral reach retrieval training, and the dominant side identified as the preferred hand for food retrieval and manipulation.

Dorsal column lesion—A laminectomy was performed to expose spinal segments C5–C8. The dura was resected to provide dorsal access to the cervical spinal cord, and unilateral electrophysiological recordings were made from dorsal rootlets to construct a

microdermatome map (Darian-Smith et al., 2000). After identification of the rootlets with receptive fields on digits 1–3, the cuneate fasciculus component of the dorsal column was cut unilaterally (within C5) level with the detectable rostral border of thumb input, using a micro scalpel (Micro-Scalpel, Feather, 15^0). The blade was marked 2mm from the tip to guide the depth of the lesion. The overlying tissue was then sutured in layers and the skin closed. Cutting the cuneate fasciculus of the dorsal column at the rostral entry of input from digit 3, ensured that lesions were as functionally comparable as possible.

DRL and DRL/DCL lesions—Dorsal rhizotomies and combined lesions were made as described above and in previous studies (Darian-Smith et al., 2013; Darian-Smith et al., 2014). For the DRL component, only rootlets with detectable cutaneous RFs on the thumb, index and middle fingers, were cut.

Craniotomy—Following the initial lesion, monkeys were allowed to recover over 9–18 weeks (see Table 2 for details of all animals used). They then underwent a second surgery during which a craniotomy was made over the central sulcus to expose the 'hand' region of the sensorimotor cortices bilaterally. Bone was removed (approximately 1 cm^2) over this area, and small windows of dura opened to expose the brain surface. Receptive fields in S1 were then mapped electrophysiologically to determine the appropriate placement of tracer injections within the 'hand' region (D1–3) of Areas 3b/1. Cortical movement was dampened, when necessary, during recording sessions using 3% agarose (in saline). This was removed prior to tracer injection.

Buprenorphine (0.01–0.02mg/kg) was administered following all surgeries as a post-operative analgesic and monkeys were returned to their cages for recovery. Within an hour animals were awake and alert and there were no sequelae. Oral buprenorphine was administered for two additional days (0.015mg/kg) and meloxicam (0.1mg/kg) for 3–5 days post-surgery, as needed.

Recordings

Recordings in dorsal root fascicles—Spinal cord receptive field mapping was used to target the lesion to the part of the cord corresponding to digits 1–3, in all animals. Importantly this made data sets comparable. In monkeys receiving a DCL only, this meant that lesions were placed rostral to the most anterior rootlet carrying detectable input from the thumb. Recordings were made from dorsal rootlets using Tungsten microelectrodes (1.2–1.4mΩ at 1 kHz; FHC) lowered vertically into them. Single or multiunit extracellular recordings were made from axons within each fascicle to produce a detailed microdermatome map (Darian-Smith et al., 2000). Cutaneous receptive fields were mapped using hand manipulation, a camel hair brush and Von Frey hairs. Receptive fields were classified as cutaneous if a stimulation force ≤ 2.0g evoked a response. For higher stimulation forces or where responses could be evoked only with joint movement or hand manipulation, the receptive field was classified as deep. If there was uncertainty about the nature of a receptive field, this was noted and for the purpose of making the lesion, it was considered cutaneous.

Cortical recordings—The somatosensory cortex was mapped in all monkeys at ~3–4 months post lesion (see Table 2), using extracellular recordings, as described for spinal cord mapping. This time period was used because previous studies in our lab have shown that cortical maps (and functional recovery) consistently take ~3 months to stabilize following deafferentation (Darian-Smith et al., 2013, 2014). At the timepoint used in this study, we had little difficulty eliciting detailed receptive field maps within S1. Whilst we sometimes observed aberrant cell discharge and there was usually clear evidence of reorganisation, it remained possible to activate cortical cells through stimulation of digits 1–3.

Cortical recordings in Areas 3b/1 allowed us to determine where input from the partially deafferented digits was localized. Tracer injections (see below) were then made bilaterally into the region of D1–3 representation in Areas 3b/1 in S1, and into the homologous region of primary motor cortex anterior to the central sulcus (Figure 1). We did not use intracortical microstimulation in M1, since this requires a different anesthetic agent, which would have prolonged surgery. However, it is well documented that digit representations are reflected across the central sulcus in primates (Penfield & Boldrey, 1937; Woolsey, 1958).

Once tracer injections were complete, the bone flap was replaced and secured using bone wax and Vetbond tissue adhesive, and the overlying incision closed.

Tracer injections

Anterograde tracers were injected into the D1–3 region of the sensorimotor cortex. This ensured that only the CST fibers most affected by the deafferentation were labeled and that injection series were comparable, as defined electrophysiologically, in the two hemispheres. Biotinylated Dextran Amine (BDA, 15% aqueous, Sigma B9139), and Lucifer Yellow Dextran (LYD, 15% aqueous, ThermoFisher D1825) were injected into M1 and S1 as indicated in Table 2. Injections were made using a constant-pressure Hamilton syringe held in a micromanipulator, with a glass micropipette (diameter ≤ 30μm) attached using fast curing (5 minute) Araldite. Injections (0.3μl) were made at a 0.8–1mm depth, and kept in place for 2 minutes post-injection. Animals were kept for ~6 weeks following the craniotomy to allow sufficient time for tracer uptake.

Perfusion and tissue processing

Following the induction of anesthesia with Ketamine, and isoflurane (see Surgical Procedures above), monkeys were given a lethal dose of sodium pentobarbital (Beuthanasia, i.v.; minimum 100mg/kg). They were then perfused through the heart with heparinised phosphate buffered saline (0.1M), followed by 4% paraformaldehyde, to fix the tissue. The brain and spinal cord were removed and postfixed for 4 hours, and cryoprotected with 30% sucrose.

The brain and spinal cord were then blocked, photographed, and flash frozen using isopentane and stored at −80C. Blocks were sectioned transversely (50μm thickness) using a freezing microtome, and collected in 24 well trays. Separate series were processed for BDA, LYD, and cresyl violet.

To visualise BDA, free floating sections were blocked for endogenous peroxidase (Bloxall, Vector labs, 10 minutes), washed in 0.1% triton in 0.1M phosphate buffer, incubated in ABC (Vector, PK-6100, 1h, room temperature), washed again, and incubated in nickel intensified diaminobenzidine (DAB) with urea peroxidase (Sigmafast, D0426) for 7–15 minutes.

LYD was visualized immunocytochemically. Sections were blocked (Bloxall, Vector labs), washed with 0.1% triton-X 100 in Tris buffered saline (0.1M TBS-TX), and then incubated with polyclonal anti-Lucifer yellow made in rabbit (Invitrogen; A5750; 1:200 dilution, RRID: AB_2536190) for 48 hours (4oC). This was washed out with TBS-TX and replaced with biotinylated anti-rabbit (Vector, BA-1000; 1:200, RRID: AB_2313606) for 24 hours. Following rinsing, avidin biotin was added to attach peroxidase (ABC kit; Vector, PK-4000) and sections reacted with 0.05% DAB with 0.01% H_2O_2 until the reaction product was clearly visible.

Tracing terminal fields and image processing

The terminal distributions of labeled axons were mapped using Neurolucida software (MBF bioscience) in combination with a Lucivid projection (MBF Bioscience). Maps were made for a series of sections, ranging from C1-T6 and separated by 400μm. Contours were drawn around the mapped boutons to outline the distribution territory and the area of this was calculated. Outlying boutons were not included if they were few in number (<5) since they constitute less than 1% of the total population.

Overall terminal field volumes were calculated (in 6 monkeys: DCL – 1401, 1403; DRL – 603, 1108; DRL/DCL – 1106, 1109), by multiplying area (within each section) by inter-section distance and section thickness.

Statistical analysis

Statistical analyses were restricted to the C6–C8 segments, for several reasons. This formed the ‘lesion zone’, or the region most affected by the deafferentation, where terminal labeling peaked and where CST terminations were present following each of the three lesion types (DRL, DCL and DRL/DCL). For sections in this region, image files were exported from Neurolucida for analysis in Fiji (Schindelin et al., 2012). The grey matter was divided into three regions (D= dorsal, M= medial, V= ventral) approximating the dorsal horn, intermediate zone and ventral horn (see Darian-Smith et al., 2014 for more details). The dorsal region was defined manually by drawing a line between the base of the midsagittal fissure and the medial border of the spinal grey at the (lateral) base of the dorsal horn. This approximated Rexed layers I–VI (Morecraft et al., 2013). The subsequent division between medial (~Rexed layer VII), and ventral areas (mainly Rexed layers VIII and IX with a small ventral portion of layer VII), was then made using a custom macro program in Fiji. Once the regions were defined, areas were calculated for each (D_1, M_1, V_1) as well as for the terminal bouton territory within them (D_2, M_2, V_2). A simple ratio of these two values then allowed us to record the percentage of each area occupied by terminal boutons (D_2/D_1, M_2/M_1, and V_2/V_1). These data were analysed as a restricted maximum likelihood (REML) mixed model in SAS 9.4 for Windows, as described below. The assumptions of mixed models (homogeneity of variance, linearity, and normality of error) were tested post-hoc, and the

data were angular transformed to meet these assumptions, as one would expect for a percentage score (Grafen & Hails, 2002).

We used a repeated measures approach to control for systematic variation between animals (Newman J, 1997), by comparing matched section position along the cord, ipsi-versus contralateral distribution patterns (relative to lesion), and the dorsal/medial/ventral regions within each section (i.e. repeated measures were made within each animal using these three variables). This approach greatly increases statistical power, despite the relatively small number of animals (Darian-Smith et al., 2014; Festing, 2014; McConway, 1992; Still, 1982). Projections from M1 and S1 cortex were analysed separately using the same model. Subject (i.e. monkey) was nested within lesion type (i.e. DRL, DCL, or DRL/DCL). Cord position was controlled for as a quadratic term (given that the relationship between the lesion and the terminal distribution was likely to be curvilinear). Section subregion (area = D, M or V), treatment (lesion type), and section side (contra-versus ipsi-lateral to the lesion) were included, and a three way interaction was used to calculate least-squares-means (LSM) and standard errors, controlled for monkey and cord position. These means were then tested using custom contrasts (F-tests) that directly assessed each of our research questions:

First, we compared each subregion (D, M, V), with the corresponding control, defined as the contralateral DRL terminal distribution area mean (Cheema, Rustioni, & Whitsel, 1984; Darian-Smith et al., 2013; Darian-Smith et al., 2014; Galea & Darian-Smith, 1997a). We also tested for overall differences from the control by combining subregions for each side of the cord. Bonferroni-corrected post-hoc tests were conducted for means against the control level. *Second*, we wanted to know whether the DRL/DCL combined lesion differed significantly from a simple sum of the effects of the DRL and DCL lesions. Following an overall test of this hypothesis, post hoc tests were performed for each combination of lesion type and section side (contralateral vs ipsilateral to lesion). *Finally*, we wanted to test whether the DCL alone differed significantly from the DRL/DCL combined lesion. Again, following an overall test of this hypothesis, we performed Bonferroni-corrected post hoc tests for each combination of lesion type and section side.

In a separate analysis (Figure 7b), we used the same statistical approach (above), but pooled data from the dorsal, medial and ventral subdivisions. The extent of terminal labeling was compared between the two sides of the spinal cord relative to the lesion, both within lesion groups and across lesion groups to determine differences. Data were collected and analysed as described above from 6 monkeys (2 from each of the three lesion groups), to create histograms showing CST terminal areas (normalized as a percentage of the spinal grey area), both ipsi-and contralateral to the lesion.

Results

The M1 and S1 corticospinal terminal territories were assessed in monkeys 4–5 months following a dorsal column lesion (within the C5 segment), and compared with animals from previous studies who had received either a DRL or a combined DRL/DCL. Only projections from D1–D3 representational fields were labeled and analysed, since these were the cortical

regions most affected by the deafferentation, and most closely associated with digit opposition and finely controlled dexterity.

Extent of dorsal column lesions

Dorsal column lesions were highly consistent between animals and limited to the cuneate fasciculus (see Figure 1a,b for DCL only and Figure 1e for DRL/DCL; Darian-Smith et al., 2014). There may have been minor sparing of the cuneate fasciculus medially, which is topographically associated with input from more radial (i.e. D5) hand regions. As such, we removed the majority of fast conducting cutaneous inputs from the digits of the ipsilateral hand, as well as the proprioceptive information, to the cuneate nucleus of the brainstem (and in turn all higher order structures). Importantly, when a DCL was made alone, the spinothalamic, spinoreticular and spinocerebellar tracts remained intact so the injury was specific to the cutaneous and proprioceptive afferents of the forelimb/hand.

Behavioral observations following a DCL alone

No formal behavioral data were collected for these animals following injury. Our observations, however, indicated an initially subtle deficit, which was most easily seen when animals performed a reach retrieval grasp task, identical to that used in earlier work (Darian-Smith & Ciferri, 2005). Though these data were insufficient to quantify, they were consistent with earlier documented reports of dorsal column injury in monkeys, where recovery largely occurred over the first 2–3 months leaving only subtle long term deficits in fine tactile discrimination and fractionation (Glendinning et al., 1992; Lassek, 1954; Leonard et al., 1992; Qi, Kaas, & Reed, 2014).

Cortical tracer injection sites

Anterograde tracer injection sites were determined using classic single or multi-unit recordings to map receptive fields and somatotopy in the region of hand representation in the S1 cortex (Area 3b/1) opposite the side of the lesion. We only injected the areas of M1 and S1 directly involved with activity in digits 1–3 of the hand. The relative placement of these injection sites are shown for both DCL animals in Figure 1C–D. Note that tracer injections were made bilaterally (Table 2).

Figure 2 shows photomicrographs of cortical injection sites, and in all cases, staining was localised to the grey matter of either Brodmann Areas 3b and 1, or the motor area 4. There was no contamination of areas across the central sulcus and tracer was not found in the underlying white matter tracts. The volume of the injected cortical area was difficult to determine, particularly for LYD which did not have sharp staining boundaries. However, we are confident that our injections were comparable across hemispheres/animals. Sites were determined electrophysiologically in both hemispheres, and equivalent injections (with respect to number of injections, volume of tracer, depth, timing, etc) were placed into regions of D1–3 representation in each hemisphere.

Projection patterns

Motor CST projections—Figure 3 shows M1 CST terminal bouton distributions within the spinal cord following a DCL alone, with extraneous labeling observed bilaterally from

C1 through T5 in both monkeys, which was ~1.5 segments (or 11–14mm) beyond that seen in uninjured animals (see also Galea and Darian-Smith, 1997a; Morecraft et al., 2013). The relative segmental extent of label was equivalent across monkeys, though the absolute rostrocaudal measure of C1 through T5 labeling differed due to normal variation in spinal cord length (i.e. M1401=53.82mm, and M1403=68.64mm). The spatial distribution (and rostrocaudal spread) of labeled terminals was similar to that seen in animals with combined DRL/DCLs (see Figures 3, 5, and 8; Darian-Smith., 2014), though it was statistically less extensive (see below and Figure 7). Labeling was significantly greater in animals with a DCL than that seen in monkeys receiving a DRL alone (Figures 3, 5, 7 and 8), with bouton fields expanding further ventral, particularly in the segments close to the lesion. It was also very common to see clusters of boutons in the dorsal horn, again, most often close to the site of injury (Figures 5b, c).

Sensory CST projections—Figure 4 shows terminal distribution patterns for S1 CSTs. Here we observed a significant bilateral expansion of the terminal territory into the intermediate zone and ventral horn. This was also similar to, but not as extensive as that seen in monkeys with a combined DRL/DCL (Darian-Smith et al., 2014). Terminal boutons were found rostrocaudally in segments extending from C1-T2 (M1401= 37.9mm, M1403= 49.7mm), or almost 1.5 segments beyond the range observed in 'normal' (i.e. labeling in DRL contralateral to the lesion) monkeys, but terminal sprouting stopped 2 segments short of the most caudal labeling observed in animals that received a combined DRL/DCL (Figures 4, 6 and 8). This was in contrast to the sharp reduction (of ~40%) of the terminal territory observed (ipsilateral to the lesion) following a DRL (Darian-Smith et al., 2013; Darian-Smith et al., 2014) where boutons were only observed between C1–C8.

Statistical analysis

A more detailed statistical analysis of terminal labeling patterns within segments C5–C8, allowed us to compare CST terminal bouton patterns between the DCL, DRL and combined lesion types (Figure 7). The goal here was *first* to compare DCL sprouting relative to control (taken as the contralateral labeling in DRL monkeys), *second* to use our DCL data to assess whether or not peripheral and central lesions interact to produce CST terminal labeling patterns, and *third* to compare DCL with DRL/DCL labeling patterns.

DCL sprouting relative to control—For motor cortex projections following a DCL alone, each of the subregions (i.e. D, M, V, on both sides of the cord) were found to differ from the control level (contralateral DRL lesion) with all P values <0.005.

For S1 CST projections, area D was not significantly different from control on either side of the cord (lesion side compared with control P=0.095; contralateral compared with control P=0.5). However, all other comparisons (except for V ipsilateral, P= 0.024 where Bonferroni = 0.0167) showed significant sprouting relative to control (M ipsilateral and M contralateral P< 0.0001, and V contralateral P< 0.0009). Bonferroni-corrected *post hoc* tests of the individual areas' difference from their respective control regions are indicated in Figure 7.

Is DRL/DCL sprouting a simple sum of DRL and DCL sprouting?—For motor cortex projections, CST sprouting following a DRL/DCL was found to be significantly lower than the simple sum of sprouting observed in DCL and DRL animals ($F_{6,10}$=202.91; P<0.0001), when all subregions (D, M, and V) and both sides of the cord were included. Bonferroni-corrected *post hoc* tests for each of the 6 regions showed that this was due to significant non-additive effects of the lesion types (DCL and DRL) in Dorsal and Medial contralateral, and Medial ipsilateral subregions (see Figure7).

Similarly, for S1 cortex projections, sprouting in DRL/DCL animals was also significantly lower than the simple sum of sprouting following DCL and DRL ($F_{6,10}$=13.39; P=0.0003), when all subregions and both sides of the cord were included. Bonferroni-corrected *post hoc* tests for each of the 6 subregions, showed that this was again due to significant non-additive effects of the lesion types (DCL and DRL), this time in the Dorsal and Medial contralateral subregions only.

Does DCL differ from DRL/DCL sprouting?—For motor cortex projections, sprouting observed after DRL/DCL was always significantly greater than that following DCL alone ($F_{6,10}$=74.77; P<0.0001). Bonferroni-corrected *post hoc* tests showed that this was due to significantly greater sprouting in all three ipsilateral subregions, as well as the Medial contralateral subregion for DRL/DCLs.

For S1 projections, sprouting following DRL/DCL was always significantly greater than that observed after a DCL ($F_{6,10}$=12.92; P=0.0003), for all subregions and sides. Bonferroni-corrected *post hoc* tests showed that this was due to significantly greater sprouting in the Dorsal ipsilateral subregion only in DRL/DCL animals.

Finally, we compared the extent of terminal labeling in the spinal cord, ipsi-and contralateral to the lesion. While these data are apparent in Figure 7a, our findings are more clearly summarized in Figure 7b. Interestingly, comparisons between M1 and S1 CSTs showed similar trends for both CST subcomponents. In DCL animals we consistently observed more extensive terminal labeling contralateral to the lesion (see Figures 4, 5, 6, and 7), while the opposite was true in DRL/DCL animals, where labeling was more extensive on the side ipsilateral to the lesion (Darian-Smith et al., 2014). This trend was consistent, however the contralateral/ipsilateral bias only reached statistical significance in S1 DRL (Darian-Smith et al., 2013) and M1 DCL groups. Though we were unable to quantify terminal bouton density differences (as different injections were made in each hemisphere), greater densities visibly corresponded to the side of greatest terminal volume, in all monkeys.

Total terminal/grey matter distribution volumes—Terminal distributions and grey matter areas were used for the statistical analyses described above, so it was straightforward to estimate total volumes for terminal labeling and grey matter to see how these varied across monkeys. Within all monkeys (n=10), we found no statistical difference in grey matter volumes on the two sides of the cord, which means there was no detectable grey matter atrophy on the side of the lesion following deafferentation, at least during the first 5–6 post-lesion months. However, it should be noted that the total volume of grey matter, and by definition the CST terminal territories, differed between monkeys, which simply reflects

the variability in cord length across individuals. For example, the two DCL monkeys used in this study were a similar age and weight (M1401 - 3.60kg, M1403 - 3.52kg) at the time of perfusion. However, their C1-T4 cord lengths differed by about 1.5cm at ~5.0cm (M1401) versus ~6.5cm (M1403). As might be expected, in M1401 the C1-T4 grey matter total volumes were also smaller at 109mm^3 (ipsilateral to the lesion), and 105mm^3 (contralateral), whereas in M1403 they were 159mm^3 (ipsilateral) and 155mm^3 (contralateral). These differences did not impact the findings of this study, but do underscore inter-animal cord size variability.

Discussion

Here we report extensive bilateral corticospinal sprouting from each of the M1 and S1 (3b/1) subcomponents of the CST 4–5 months following a DCL. This response was similar to the M1 and S1 CST terminal sprouting observed following a combined DRL/DCL (Darian-Smith et al., 2014), though less extensive. Our findings demonstrate that even a small central DCL is sufficient to induce expansive bilateral terminal sprouting of spared M1 and S1 CSTs to the cervical, and thoracic spinal cord. Our findings strongly suggest that the immune response induced following a central injury (but not a peripheral lesion), is critically important in providing a permissive environment for such sprouting. Additionally our new findings now show that the pattern of terminal labeling observed following the combined DRL/DCL injury is not equal to the sum effect of the peripheral and central injuries. Rather, it involves a complex nonlinear interaction between them, though the basis of this interaction is not understood.

Context

A number of factors should be considered as context for this work. *First*, the lesions described in this study were intentionally small and precisely defined, so that the relative involvement of the peripheral and central components could be determined. This contrasts with typical clinical SCIs, which are highly variable, and which can involve larger areas of the cord, and both central and peripheral structures. *Second*, we did not extend our statistical analyses beyond segments C6–C8 in this study. The rationale was that this was the region of the cord most directly deafferented by the lesions used, and the region most clearly involved in hand function, and recovery. *Third*, the hemisphere of origin for the bilateral CST sprouting could not be determined since tracers were injected in an identical configuration in both hemispheres. In contrast to the M1 CST, the S1 CST does not project ipsilaterally in normal animals (Cheema et al., 1984; Galea & Darian-Smith, 1997a), making the bilateral aspect of the S1 CST sprouting particularly curious.

Clearly the loss of primary afferent activation of spinal and cortical neurons was a primary contributor to pathway reorganization and CST sprouting in our monkeys. However, since the DRL (which resulted in the loss of CST input from the side of the lesion), removed more primary afferent information than a DCL (which led to considerable bilateral CST sprouting), the differences in the CST response between the different lesion groups necessarily involved additional factors.

The extensive CST sprouting demonstrated following a DCL alone, underscores the importance of the central injury in the induction of this axon terminal growth. This was a missing element in our earlier work, and our findings now firmly implicate the central inflammatory and immune response in providing a permissive environment following a central injury. Relative to peripheral injuries (e.g. DRL), the immune response is greatly enhanced following a CNS lesion (e.g. DCL), though the details of this complex process remain poorly understood, particularly in primates. However, there are well known acute, sub-chronic and chronic response phases, and an initial massive proliferation of astrocytes and microglia that help form a glial scar (Karimi-Abdolrezaee & Billakanti, 2012). These, as well as other cell types and supporting elements (e.g. oligodendroglia, macrophages, pericytes, neutrophils, perineuronal nets, etc), contribute to a dynamic and changing cellular and molecular environment, both at the site of a CNS injury (e.g. stroke) and to varying degrees, well beyond (Nagamoto-Combs, McNeal, Morecraft, & Combs, 2007; Nagamoto-Combs, Morecraft, Darling, & Combs, 2010). Many of these changes provide support for and even enhance neuronal repair (Ahmed, Patil, & Agrawal, 2017; Liddelow & Barres, 2017), while others have been shown to inhibit axonal growth following spinal cord (Fabes et al., 2006; Fitch & Silver, 2008; Sorg et al., 2016; Ulndreaj et al., 2017), and other CNS injuries (Raposo & Schwartz, 2014).

While we have no direct evidence of inflammatory changes in our central models of SCI, previous work has shown proliferation of activated astrocytes localized to the spinal lesion zone in monkeys following DRL (Vessal, Aycock, Garton, Ciferri, & Darian-Smith, 2007). This response was specific to the side of the lesion, had outlasted the acute phase (animals were 1.5–2 months post injury) and also correlated with similar changes in sensorimotor cortex (Vessal & Darian-Smith, 2010). Clearly more work is needed to investigate the different immune activity associated with peripheral and central injuries, such as those defined in the current study, to ascertain factors enabling the CST sprouting following a DCL or DRL/DCL versus a DRL.

Anatomical bases for bilateral M1 CST sprouting

In this study M1 CST sprouting extended beyond normal range within the intermediate zone and ventral horn, and from C1 through T5 following a DCL alone, which was 1.5 segments beyond that seen in uninjured monkeys. This represents an impressive bilateral spontaneous reorganization prompted by a small central injury.

Candidate pathways that could help drive M1 CST bilateral sprouting include transcallosal, ipsilateral CST and/or brainstem projections, as well as propriospinal and commissural interneurons within the cord. Current evidence is weak, or inconsistent for transcallosal pathways playing a major role. Connections between M1 hand representations are modest in normal animals (Jenny, 1979; Rouiller et al., 1994), and while some studies in SCI and stroke patients report increased communication between the two hemispheres (Lundell et al., 2011; Ward, Brown, Thompson, & Frackowiak, 2003), others suggest an opposite effect (Bunday & Perez, 2012). Ipsilateral cortico-cortical pathways may also play a role in the induction of CST sprouting, but their influence is likely to be minimal (Kambi, Tandon,

Mohammed, Lazar, & Jain, 2011), and would not explain the observed disparities in responses between the lesion groups.

Ipsilateral M1 CST projections (Kuypers, 1981) comprise ~2% of the CST from the M1 hand/arm region in normal monkeys (Morecraft et al., 2013). The role of this projection remains unclear (Soteropoulos, Edgley, & Baker, 2011), though it has been implicated in recovery following spinal injury (Galea & Darian-Smith, 1997a; Nishimura et al., 2007; Rosenzweig et al., 2009), and may also be adaptive in this study, by providing a pathway to the lesioned side below the lesion.

The brainstem reticular formation, which receives collateral CST input and which gives rise to the reticulospinal tract, may also mediate the bilateral response. This projection can innervate intrinsic hand muscles in healthy monkeys (Soteropoulos, Williams, & Baker, 2012) and is enhanced following corticospinal injury (Zaaimi, Edgley, Soteropoulos, & Baker, 2012). Premotor, and SMA cortices, which have greater input to the reticular formation than M1 (Fregosi, Contestabile, Hamadjida, & Rouiller, 2017), may also shape reticulospinal output, and influence bilateral CST sprouting.

Spinal commissural interneurons are also well placed to contribute to compensatory CST sprouting. This diverse group of cells receive input from the major descending motor centers in cortex as well as from peripheral afferents, and studies in cats show that they exert influence over a range of contralateral postsynaptic targets (Jankowska, 2008). The network is complex and though progress has been made in terms of genetic identification of some subclasses of commissural interneurons in mice (Gosgnach et al., 2017), and in characterising functional connectivity in the cat (Jankowska, 2008), little is known about their role in primates (Soteropoulos, Edgley, & Baker, 2013).

Lastly, the intraspinal propriospinal network has been implicated in recovery following SCI (Flynn, Graham, Galea, & Callister, 2011; Isa, 2017; Kinoshita et al., 2012; Tohyama et al., 2017). Here, the C3–4 propriospinal system loses its normal primary afferent input from the digits and hand. In response to this, and following the central DCL (and DRL/DCL), but not the DRL alone, we observed indirect support for PN involvement in an upswing in both M1 and S1 CST sprouting in the rostral cervical segments including C3–4 (Figures 3, 4 and 8). It is important to note, however, that whilst the PN has been shown to contribute to reaching in cats (Alstermark, Lundberg, Norrsell, & Sybirska, 1981) and hand function in non-human primates (Isa, Ohki, Seki, & Alstermark, 2006; Kinoshita et al., 2012; Tohyama et al., 2017), evidence for a role in humans is more controversial (Pierrot-Deseilligny, 1996).

Anatomical bases for bilateral S1 CST sprouting

The S1 CST also sprouted extensively and bilaterally in monkeys that received a small DCL in the present study. These projections extended ventrally within the grey matter, and from C1 through T2, or ~1.5 segments beyond the range observed in normal (Figures 3 and 4) monkeys. This was, however, 2 segments short of the most caudal labeling observed in animals that received a combined DRL/DCL (see Figures 4, 7, and 8).

Few obvious neuronal pathways exist to drive the bilateral S1 CST sprouting observed following a DCL. Transcallosal fibres connecting S1 hand regions in healthy primates are even more sparse than for M1 (Jones & Powell, 1969; Killackey, Gould, Cusick, Pons, & Kaas, 1983), though significant transcallosal connections between areas 2 and 5 (Iwamura, Taoka, & Iriki, 2001), could feed back to the Area 3b/1 hand region.

Unlike the M1 CST, the S1 CST extends few if any collateral branches across the midline in the cervical cord in normal animals, and there is little evidence that this changes significantly following spinal injury either in this or past investigations (see Figure 6c for rare example of crossing fibers; Darian-Smith et al, 2013; Darian-Smith et al, 2014). However, the primary somatosensory cortex does project bilaterally to the brainstem reticular formation in our monkeys (Fisher and Darian-Smith, unpublished), which in turn could drive reticulospinal input to help shape the bilateral sprouting observed.

What is the role of CST terminal sprouting?

Our findings raise key questions. Why does a combined DRL/DCL induce more CST sprouting than a DCL alone, and what is the mechanistic basis for the interaction between peripheral and central lesions? We also have yet to determine if other affected CST subdivisions (e.g. premotor, posterior parietal) sprout following a central or combined spinal injury, to contribute to the recovery process.

What is the relationship between CST sprouting and functional recovery? Our findings, to date, demonstrate that the extent of the CST sprouting does not clearly track with behavioral recovery following SCI. That is, a DRL produces a far more extreme behavioral deficit and recovery than a DCL, yet it results in little M1 CST terminal sprouting and a 40% retraction of S1 CST terminals within the cord (Darian-Smith et al., 2013). In contrast, a DCL on its own (which produces only a subtle initial deficit and recovery), and a combined DRL/DCL (which produces a deficit and recovery similar to the DRL alone), both induce extensive bilateral M1 and S1 CST sprouting. This is important because CST sprouting has long been used as a biomarker of recovery in SCI research, and many studies simply aim to enhance this process globally without fully considering the underlying mechanisms at play. Clearly more work is needed to understand this complicated process, and the relationship between CST sprouting and functional recovery.

Acknowledgments

We would like to thank Jerome Geronimo for his technical assistance with the analysis software. This work was supported by the National Institute of Neurological Disorders and Stroke (R01 NS048425 and R01 NS091031 to CD-S).

References

Ahmed A, Patil AA, Agrawal DK. 2017; Immunobiology of spinal cord injuries and potential therapeutic approaches. Mol Cell Biochem. doi: 10.1007/s11010-017-3184-9

Alstermark B, Lundberg A, Norrsell U, Sybirska E. 1981; Integration in descending motor pathways controlling the forelimb in the cat. 9. Differential behavioural defects after spinal cord lesions interrupting defined pathways from higher centres to motoneurones. Exp Brain Res. 42(3–4):299–318. [PubMed: 7238672]

Bunday KL, Perez MA. 2012; Impaired crossed facilitation of the corticospinal pathway after cervical spinal cord injury. J Neurophysiol. 107(10):2901–2911. DOI: 10.1152/jn.00850.2011 [PubMed: 22357796]

Carmel JB, Kimura H, Berrol LJ, Martin JH. 2013; Motor cortex electrical stimulation promotes axon outgrowth to brain stem and spinal targets that control the forelimb impaired by unilateral corticospinal injury. Eur J Neurosci. 37(7):1090–1102. DOI: 10.1111/ejn.12119 [PubMed: 23360401]

Cheema SS, Rustioni A, Whitsel BL. 1984; Light and electron microscopic evidence for a direct corticospinal projection to superficial laminae of the dorsal horn in cats and monkeys. J Comp Neurol. 225(2):276–290. DOI: 10.1002/cne.902250211 [PubMed: 6547152]

Darian-Smith C, Brown S. 2000; Functional changes at periphery and cortex following dorsal root lesions in adult monkeys. Nat Neurosci. 3(5):476–481. DOI: 10.1038/74852 [PubMed: 10769388]

Darian-Smith C, Ciferri MM. 2005; Loss and recovery of voluntary hand movements in the macaque following a cervical dorsal rhizotomy. J Comp Neurol. 491(1):27–45. DOI: 10.1002/cne.20686 [PubMed: 16127695]

Darian-Smith C, Lilak A, Alarcon C. 2013; Corticospinal sprouting occurs selectively following dorsal rhizotomy in the macaque monkey. J Comp Neurol. 521(10):2359–2372. DOI: 10.1002/cne.23289 [PubMed: 23239125]

Darian-Smith C, Lilak A, Garner J, Irvine KA. 2014; Corticospinal sprouting differs according to spinal injury location and cortical origin in macaque monkeys. J Neurosci. 34(37):12267–12279. DOI: 10.1523/jneurosci.1593-14.2014 [PubMed: 25209269]

Dum RP, Strick PL. 1991; The origin of corticospinal projections from the premotor areas in the frontal lobe. J Neurosci. 11(3):667–689. [PubMed: 1705965]

Fabes J, Anderson P, Yanez-Munoz RJ, Thrasher A, Brennan C, Bolsover S. 2006; Accumulation of the inhibitory receptor EphA4 may prevent regeneration of corticospinal tract axons following lesion. Eur J Neurosci. 23(7):1721–1730. DOI: 10.1111/j.1460-9568.2006.04704.x [PubMed: 16623828]

Festing MF. 2014; Randomized block experimental designs can increase the power and reproducibility of laboratory animal experiments. Ilar j. 55(3):472–476. DOI: 10.1093/ilar/ilu045 [PubMed: 25541548]

Fitch MT, Silver J. 2008; CNS injury, glial scars, and inflammation: Inhibitory extracellular matrices and regeneration failure. Exp Neurol. 209(2):294–301. DOI: 10.1016/j.expneurol.2007.05.014 [PubMed: 17617407]

Flynn JR, Graham BA, Galea MP, Callister RJ. 2011; The role of propriospinal interneurons in recovery from spinal cord injury. Neuropharmacology. 60(5):809–822. DOI: 10.1016/j.neuropharm.2011.01.016 [PubMed: 21251920]

Fregosi M, Contestabile A, Hamadjida A, Rouiller EM. 2017; Corticobulbar projections from distinct motor cortical areas to the reticular formation in macaque monkeys. Eur J Neurosci. 45(11):1379–1395. DOI: 10.1111/ejn.13576 [PubMed: 28394483]

Friedli L, Rosenzweig ES, Barraud Q, Schubert M, Dominici N, Awai L, … Courtine G. 2015; Pronounced species divergence in corticospinal tract reorganization and functional recovery after lateralized spinal cord injury favors primates. Sci Transl Med. 7(302):302ra134.doi: 10.1126/scitranslmed.aac5811

Galea MP, Darian-Smith I. 1994; Multiple corticospinal neuron populations in the macaque monkey are specified by their unique cortical origins, spinal terminations, and connections. Cereb Cortex. 4(2):166–194. [PubMed: 8038567]

Galea MP, Darian-Smith I. 1997a; Corticospinal projection patterns following unilateral section of the cervical spinal cord in the newborn and juvenile macaque monkey. J Comp Neurol. 381(3):282–306. [PubMed: 9133569]

Galea MP, Darian-Smith I. 1997b; Manual dexterity and corticospinal connectivity following unilateral section of the cervical spinal cord in the macaque monkey. J Comp Neurol. 381(3):307–319. [PubMed: 9133570]

Glendinning DS, Cooper BY, Vierck CJ Jr, Leonard CM. 1992; Altered precision grasping in stumptail macaques after fasciculus cuneatus lesions. Somatosens Mot Res. 9(1):61–73. [PubMed: 1595322]

Gosgnach S, Bikoff JB, Dougherty KJ, El Manira A, Lanuza GM, Zhang Y. 2017; Delineating the Diversity of Spinal Interneurons in Locomotor Circuits. J Neurosci. 37(45):10835–10841. DOI: 10.1523/jneurosci.1829-17.2017 [PubMed: 29118212]

Grafen, A, Hails, R. Modern statistics for the life sciences. Oxford University Press; 2002.

Isa T. 2017; The Brain Is Needed to Cure Spinal Cord Injury. Trends Neurosci. 40(10):625–636. DOI: 10.1016/j.tins.2017.08.002 [PubMed: 28893422]

Isa T, Ohki Y, Seki K, Alstermark B. 2006; Properties of propriospinal neurons in the C3–C4 segments mediating disynaptic pyramidal excitation to forelimb motoneurons in the macaque monkey. J Neurophysiol. 95(6):3674–3685. DOI: 10.1152/jn.00103.2005 [PubMed: 16495365]

Iwamura Y, Taoka M, Iriki A. 2001; Bilateral activity and callosal connections in the somatosensory cortex. Neuroscientist. 7(5):419–429. [PubMed: 11597101]

Jain N, Qi HX, Collins CE, Kaas JH. 2008; Large-scale reorganization in the somatosensory cortex and thalamus after sensory loss in macaque monkeys. J Neurosci. 28(43):11042–11060. DOI: 10.1523/jneurosci.2334-08.2008 [PubMed: 18945912]

Jankowska E. 2008; Spinal interneuronal networks in the cat: elementary components. Brain Res Rev. 57(1):46–55. DOI: 10.1016/j.brainresrev.2007.06.022 [PubMed: 17884173]

Jenny AB. 1979; Commissural projections of the cortical hand motor area in monkeys. J Comp Neurol. 188(1):137–145. DOI: 10.1002/cne.901880111 [PubMed: 115906]

Jiang YQ, Zaaimi B, Martin JH. 2016; Competition with Primary Sensory Afferents Drives Remodeling of Corticospinal Axons in Mature Spinal Motor Circuits. J Neurosci. 36(1):193–203. DOI: 10.1523/jneurosci.3441-15.2016 [PubMed: 26740661]

Jones EG, Powell TP. 1969; Connexions of the somatic sensory cortex of the rhesus monkey. II. Contralateral cortical connexions. Brain. 92(4):717–730. [PubMed: 4983244]

Kambi N, Halder P, Rajan R, Arora V, Chand P, Arora M, Jain N. 2014; Large-scale reorganization of the somatosensory cortex following spinal cord injuries is due to brainstem plasticity. Nat Commun. 5:3602.doi: 10.1038/ncomms4602 [PubMed: 24710038]

Kambi N, Tandon S, Mohammed H, Lazar L, Jain N. 2011; Reorganization of the primary motor cortex of adult macaque monkeys after sensory loss resulting from partial spinal cord injuries. J Neurosci. 31(10):3696–3707. DOI: 10.1523/jneurosci.5187-10.2011 [PubMed: 21389224]

Karimi-Abdolrezaee S, Billakanti R. 2012; Reactive astrogliosis after spinal cord injury-beneficial and detrimental effects. Mol Neurobiol. 46(2):251–264. DOI: 10.1007/s12035-012-8287-4 [PubMed: 22684804]

Killackey HP, Gould HJ 3rd, Cusick CG, Pons TP, Kaas JH. 1983; The relation of corpus callosum connections to architectonic fields and body surface maps in sensorimotor cortex of new and old world monkeys. J Comp Neurol. 219(4):384–419. DOI: 10.1002/cne.902190403 [PubMed: 6643713]

Kinoshita M, Matsui R, Kato S, Hasegawa T, Kasahara H, Isa K, … Isa T. 2012; Genetic dissection of the circuit for hand dexterity in primates. Nature. 487(7406):235–238. DOI: 10.1038/nature11206 [PubMed: 22722837]

Kuypers HGJM. 1981Anatomy of the descending pathways.

Lassek AM. 1954; Motor deficits produced by posterior rhizotomy versus section of the dorsal funiculus. Neurology. 4:120–123. [PubMed: 13165873]

Lawrence DG, Kuypers HG. 1968; The functional organization of the motor system in the monkey. I. The effects of bilateral pyramidal lesions. Brain. 91(1):1–14. [PubMed: 4966862]

Leonard CM, Glendinning DS, Wilfong T, Cooper BY, Vierck CJ Jr. 1992; Alterations of natural hand movements after interruption of fasciculus cuneatus in the macaque. Somatosens Mot Res. 9(1): 75–89. [PubMed: 1595323]

Liddelow SA, Barres BA. 2017; Reactive Astrocytes: Production, Function, and Therapeutic Potential. Immunity. 46(6):957–967. DOI: 10.1016/j.immuni.2017.06.006 [PubMed: 28636962]

Lindau NT, Banninger BJ, Gullo M, Good NA, Bachmann LC, Starkey ML, Schwab ME. 2014; Rewiring of the corticospinal tract in the adult rat after unilateral stroke and anti-Nogo-A therapy. Brain. 137(Pt 3):739–756. DOI: 10.1093/brain/awt336 [PubMed: 24355710]

Lundell H, Christensen MS, Barthelemy D, Willerslev-Olsen M, Biering-Sorensen F, Nielsen JB. 2011; Cerebral activation is correlated to regional atrophy of the spinal cord and functional motor

disability in spinal cord injured individuals. Neuroimage. 54(2):1254–1261. DOI: 10.1016/j.neuroimage.2010.09.009 [PubMed: 20851198]

McConway, K. The number of subjects in animal behaviour experiments: Is Still still right?. Dawkins, MS, Gosling, M, editorsAcademic Press for the Association for the Study of Animal Behaviour and the Animal Behavior Society; 1992.

Morecraft RJ, Ge J, Stilwell-Morecraft KS, McNeal DW, Pizzimenti MA, Darling WG. 2013; Terminal distribution of the corticospinal projection from the hand/arm region of the primary motor cortex to the cervical enlargement in rhesus monkey. J Comp Neurol. 521(18):4205–4235. DOI: 10.1002/cne.23410 [PubMed: 23840034]

Murphy BA, Haavik Taylor H, Wilson SA, Knight JA, Mathers KM, Schug S. 2003; Changes in median nerve somatosensory transmission and motor output following transient deafferentation of the radial nerve in humans. Clin Neurophysiol. 114(8):1477–1488. [PubMed: 12888031]

Nagamoto-Combs K, McNeal DW, Morecraft RJ, Combs CK. 2007; Prolonged microgliosis in the rhesus monkey central nervous system after traumatic brain injury. J Neurotrauma. 24(11):1719–1742. DOI: 10.1089/neu.2007.0377 [PubMed: 18001202]

Nagamoto-Combs K, Morecraft RJ, Darling WG, Combs CK. 2010; Long-term gliosis and molecular changes in the cervical spinal cord of the rhesus monkey after traumatic brain injury. J Neurotrauma. 27(3):565–585. DOI: 10.1089/neu.2009.0966 [PubMed: 20030560]

Nishimura Y, Onoe H, Morichika Y, Perfiliev S, Tsukada H, Isa T. 2007; Time-dependent central compensatory mechanisms of finger dexterity after spinal cord injury. Science. 318(5853):1150–1155. DOI: 10.1126/science.1147243 [PubMed: 18006750]

Penfield W, Boldrey E. 1937; Somatic motor and sensory representation in the cerebral cortex of man as studied by electrical stimulation. Brain. 60(4):389–443.

Pierrot-Deseilligny E. 1996; Transmission of the cortical command for human voluntary movement through cervical propriospinal premotoneurons. Prog Neurobiol. 48(4–5):489–517. [PubMed: 8804118]

Qi HX, Chen LM, Kaas JH. 2011; Reorganization of somatosensory cortical areas 3b and 1 after unilateral section of dorsal columns of the spinal cord in squirrel monkeys. J Neurosci. 31(38):13662–13675. DOI: 10.1523/jneurosci.2366-11.2011 [PubMed: 21940457]

Qi HX, Gharbawie OA, Wynne KW, Kaas JH. 2013; Impairment and recovery of hand use after unilateral section of the dorsal columns of the spinal cord in squirrel monkeys. Behav Brain Res. 252:363–376. DOI: 10.1016/j.bbr.2013.05.058 [PubMed: 23747607]

Qi HX, Kaas JH, Reed JL. 2014; The reactivation of somatosensory cortex and behavioral recovery after sensory loss in mature primates. Front Syst Neurosci. 8:84.doi: 10.3389/fnsys.2014.00084 [PubMed: 24860443]

Raposo C, Schwartz M. 2014; Glial scar and immune cell involvement in tissue remodeling and repair following acute CNS injuries. Glia. 62(11):1895–1904. DOI: 10.1002/glia.22676 [PubMed: 24756949]

Rosenzweig ES, Brock JH, Culbertson MD, Lu P, Moseanko R, Edgerton VR, … Tuszynski MH. 2009; Extensive spinal decussation and bilateral termination of cervical corticospinal projections in rhesus monkeys. J Comp Neurol. 513(2):151–163. DOI: 10.1002/cne.21940 [PubMed: 19125408]

Rosenzweig ES, Courtine G, Jindrich DL, Brock JH, Ferguson AR, Strand SC, … Tuszynski MH. 2010; Extensive spontaneous plasticity of corticospinal projections after primate spinal cord injury. Nat Neurosci. 13(12):1505–1510. DOI: 10.1038/nn.2691 [PubMed: 21076427]

Rouiller EM, Babalian A, Kazennikov O, Moret V, Yu XH, Wiesendanger M. 1994; Transcallosal connections of the distal forelimb representations of the primary and supplementary motor cortical areas in macaque monkeys. Exp Brain Res. 102(2):227–243. [PubMed: 7705502]

Sainburg RL, Poizner H, Ghez C. 1993; Loss of proprioception produces deficits in interjoint coordination. J Neurophysiol. 70(5):2136–2147. [PubMed: 8294975]

Schindelin J, Arganda-Carreras I, Frise E, Kaynig V, Longair M, Pietzsch T, … Cardona A. 2012; Fiji: an open-source platform for biological-image analysis. Nat Methods. 9(7):676–682. DOI: 10.1038/nmeth.2019 [PubMed: 22743772]

Sorg BA, Berretta S, Blacktop JM, Fawcett JW, Kitagawa H, Kwok JC, Miquel M. 2016; Casting a Wide Net: Role of Perineuronal Nets in Neural Plasticity. J Neurosci. 36(45):11459–11468. DOI: 10.1523/jneurosci.2351-16.2016 [PubMed: 27911749]

Soteropoulos DS, Edgley SA, Baker SN. 2011; Lack of evidence for direct corticospinal contributions to control of the ipsilateral forelimb in monkey. J Neurosci. 31(31):11208–11219. DOI: 10.1523/jneurosci.0257-11.2011 [PubMed: 21813682]

Soteropoulos DS, Edgley SA, Baker SN. 2013; Spinal commissural connections to motoneurons controlling the primate hand and wrist. J Neurosci. 33(23):9614–9625. DOI: 10.1523/jneurosci.0269-13.2013 [PubMed: 23739958]

Soteropoulos DS, Williams ER, Baker SN. 2012; Cells in the monkey ponto-medullary reticular formation modulate their activity with slow finger movements. J Physiol. 590(Pt 16):4011–4027. DOI: 10.1113/jphysiol.2011.225169 [PubMed: 22641776]

Still AW. 1982; On the number of subjects used in animal behaviour experiments. Animal Behaviour. 30(3):873–870.

Tohyama T, Kinoshita M, Kobayashi K, Isa K, Watanabe D, Kobayashi K, … Isa T. 2017; Contribution of propriospinal neurons to recovery of hand dexterity after corticospinal tract lesions in monkeys. Proc Natl Acad Sci U S A. 114(3):604–609. DOI: 10.1073/pnas.1610787114 [PubMed: 28049844]

Ulndreaj A, Tzekou A, Mothe AJ, Siddiqui AM, Dragas R, Tator CH, … Fehlings MG. 2017; Characterization of the Antibody Response after Cervical Spinal Cord Injury. J Neurotrauma. 34(6):1209–1226. DOI: 10.1089/neu.2016.4498 [PubMed: 27775474]

Vessal M, Aycock A, Garton MT, Ciferri M, Darian-Smith C. 2007; Adult neurogenesis in primate and rodent spinal cord: comparing a cervical dorsal rhizotomy with a dorsal column transection. Eur J Neurosci. 26(10):2777–2794. DOI: 10.1111/j.1460-9568.2007.05871.x [PubMed: 18001275]

Vessal M, Darian-Smith C. 2010; Adult neurogenesis occurs in primate sensorimotor cortex following cervical dorsal rhizotomy. J Neurosci. 30(25):8613–8623. DOI: 10.1523/jneurosci.5272-09.2010 [PubMed: 20573907]

Ward NS, Brown MM, Thompson AJ, Frackowiak RS. 2003; Neural correlates of outcome after stroke: a cross-sectional fMRI study. Brain. 126(Pt 6):1430–1448. [PubMed: 12764063]

Weidner N, Ner A, Salimi N, Tuszynski MH. 2001; Spontaneous corticospinal axonal plasticity and functional recovery after adult central nervous system injury. Proc Natl Acad Sci U S A. 98(6):3513–3518. DOI: 10.1073/pnas.051626798 [PubMed: 11248109]

Woolsey, CN. Organisation of somatic sensory and motor areas of the cerebral cortex. In: Harlow, HF, Woolsey, CN, editorsBiological and biochemical bases of behaviour. University of Wisconsin Press; 1958.

Zaaimi B, Edgley SA, Soteropoulos DS, Baker SN. 2012; Changes in descending motor pathway connectivity after corticospinal tract lesion in macaque monkey. Brain. 135(Pt 7):2277–2289. DOI: 10.1093/brain/aws115 [PubMed: 22581799]

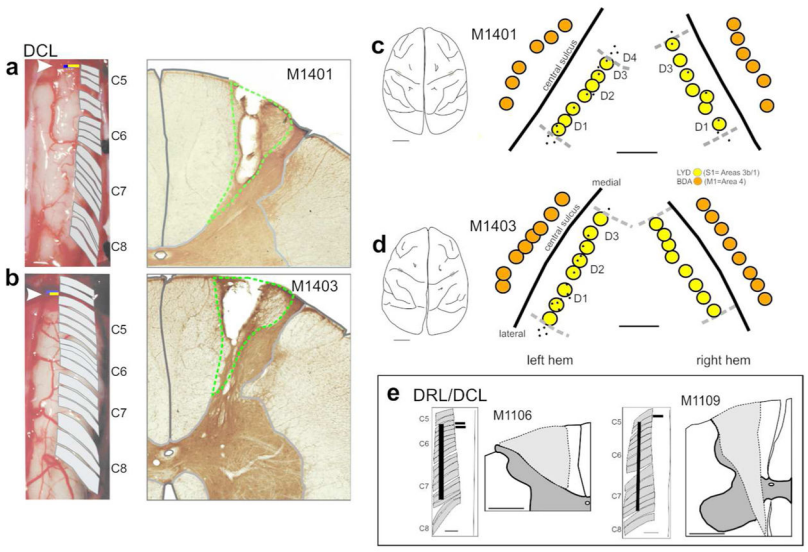

Figure 1.

Dorsal column lesions and placement of anterograde tracer injections into somatosensory and motor cortex in DCL monkeys. (**a, b**) Photographs of the spinal cord exposure for M1401 and M1403, showing the location of dorsal rootlets (C5–C8) and the dorsal column lesion (yellow bar indicated by arrowhead). The DCL was made in C5 at the rostral border of D1 input, which was mapped electrophysiologically. Adjacent photomicrographs show the DCL lesion core. Green dotted lines delineate the lesion extent, which was confined to the cuneate fasciculus of the dorsal column in both cases. **(c, d)** Tracings of brain photographs showing recording sites (black dots) and placement of tracer injections in monkeys M1401 (**c**) and M1403 (**d**). Note that no recordings were made in the right hemisphere of monkey 1403 for technical reasons. Injections into cortex on this side were therefore placed according to recordings made from left S1. LYD injections were made into somatosensory cortex (yellow) and BDA injections into motor cortex (orange). Scale bars = 1cm for brain outlines, and 1mm for injection placement. **e** Insert shows lesion extent for combined lesion monkeys M1106 and M1109, for direct comparison with DCL animals. See Darian-Smith et al., 2014 for additional information on these animals.

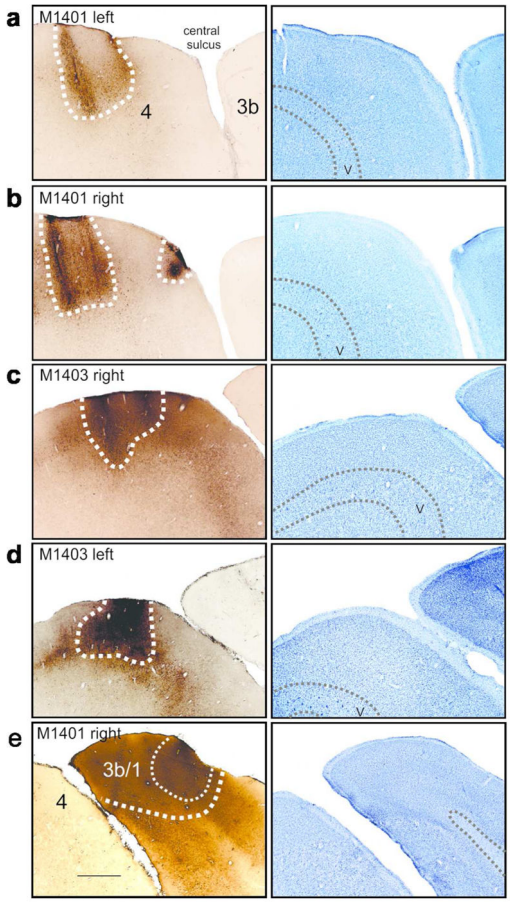

Figure 2.

Photographs of cortical injection sites. **a–d** shows BDA injection sites in M1 and **e** shows an example of an LYD injection site made in M1401. Dotted lines represent the core of each injection site. Right column shows adjacent sections stained with cresyl violet. Scale bar = 1mm

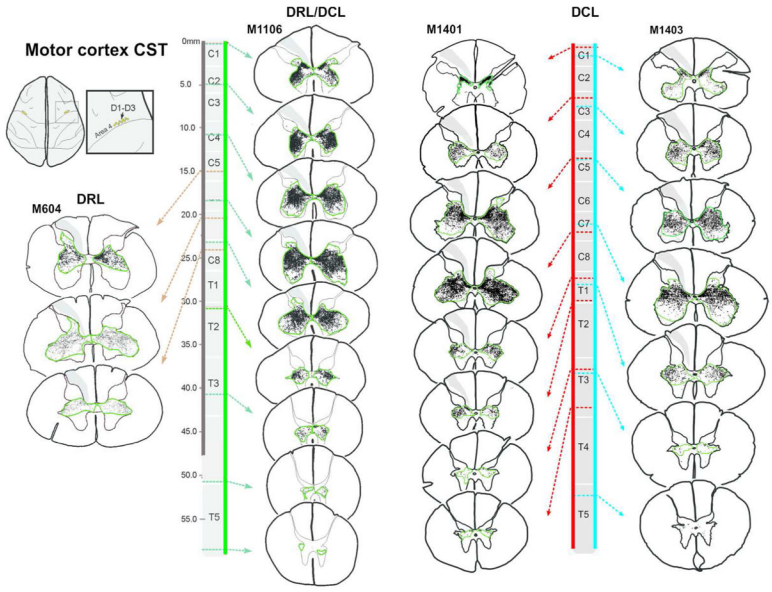

Figure 3.

Corticospinal terminal labeling in segments C1-T5, originating from primary motor cortex (digits 1–3 representation). Terminal distribution sequences for animals receiving a DRL or DRL/DCL (previously published: Darian-Smith et al., 2014), provides a direct comparison between the three different lesions. Terminal bouton distributions following a DCL lesion (M1401 and M1403), lie between the DRL and DRL/DCL terminal patterns, but are not a direct summation of the DRL and DRL/DCLs. The location of each section is indicated by dotted arrows. Color bars (black, green, red and blue) show the rostrocaudal extent of terminal bouton labeling in each case. Green contours outline the bouton distributions. The lesion is always to the left.

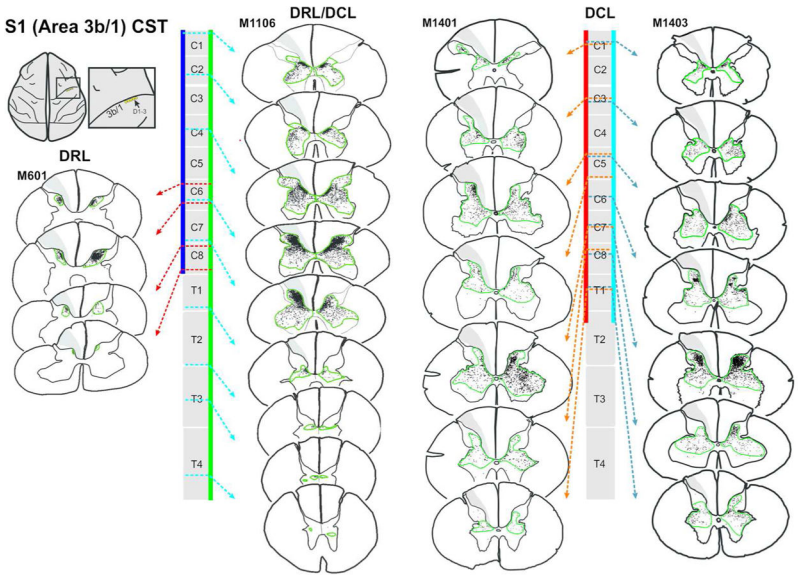

Figure 4.

Corticospinal terminal labeling in segments C1-T4, originating from primary somatosensory cortex (digits 1–3 representation). Terminal distribution sequences for animals receiving a DRL or DRL/DCL (previously published: Darian-Smith et al., 2014), allow for a direct comparison between the three different lesions. Terminal bouton distributions shown following a DCL lesion, again show a pattern that is not the sum of the DRL and DRL/DCL terminal distributions, but which is closer to that observed following a combined DRL/DCL. The location of each section along the rostrocaudal extent of the spinal cord is indicated by dotted arrows. Color bars (blue, green, red and light blue) show the rostrocaudal extent of terminal labeling in each case. Green contours outline bouton distributions. The lesion is to the left.

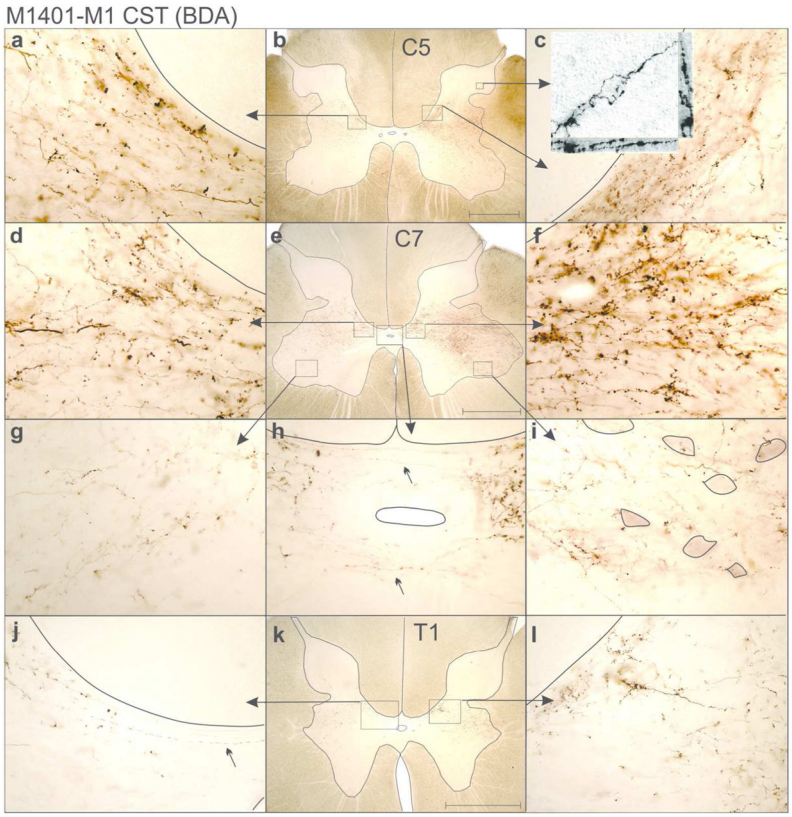

Figure 5.

Photomicrographs showing examples of M1 CST terminal labeling within the spinal grey matter of M1401, following a DCL. **a–c** show terminal labeling in a C5 section. Insert in **C** shows a confocal transmitted light Z-stack image (Nikon A1R) of sprouted axon terminals within the dorsal horn. **a** and **c** show dense terminal labeling in Rexed laminae VI/VII. **d–i** shows labeling within a C7 section. Note dense boutons extending into Rexed lamina IX, where motoneurons are outlined (**g**). **h** shows axons crossing the midline. Terminal labeling is still extensive in T1 (**j–l**), but lessens relative to C8 sections. Rexed laminae defined according to Kuypers (1981), and Morecraft et al. (2013). Lesion is to the left. Scale bars = 1 mm.

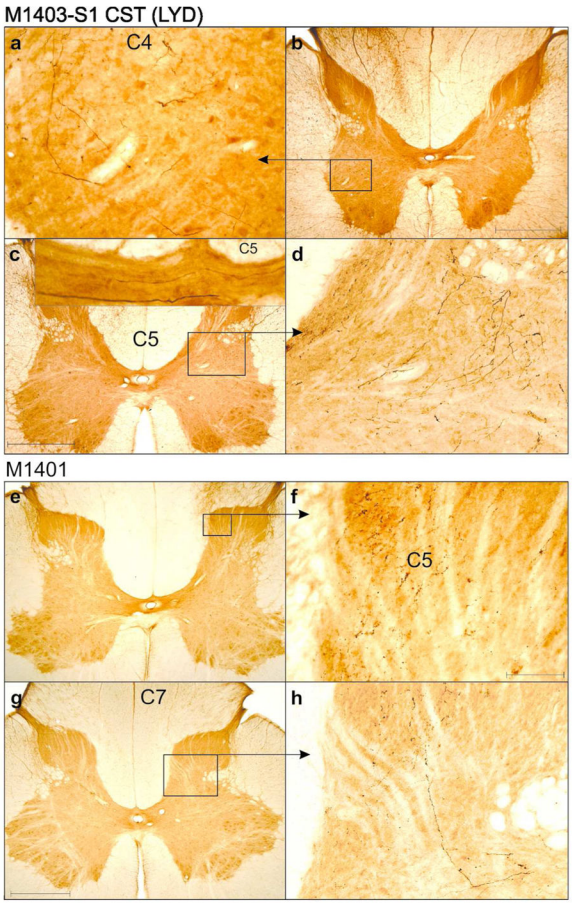

Figure 6.

Photomicrographs showing examples of S1 CST terminal labeling within the spinal grey matter of M1401 and M1403, following a DCL. Inset in **c** shows rare midline crossing axons although these have no visible boutons. Lesion is to the left. Scale bars = 1 mm

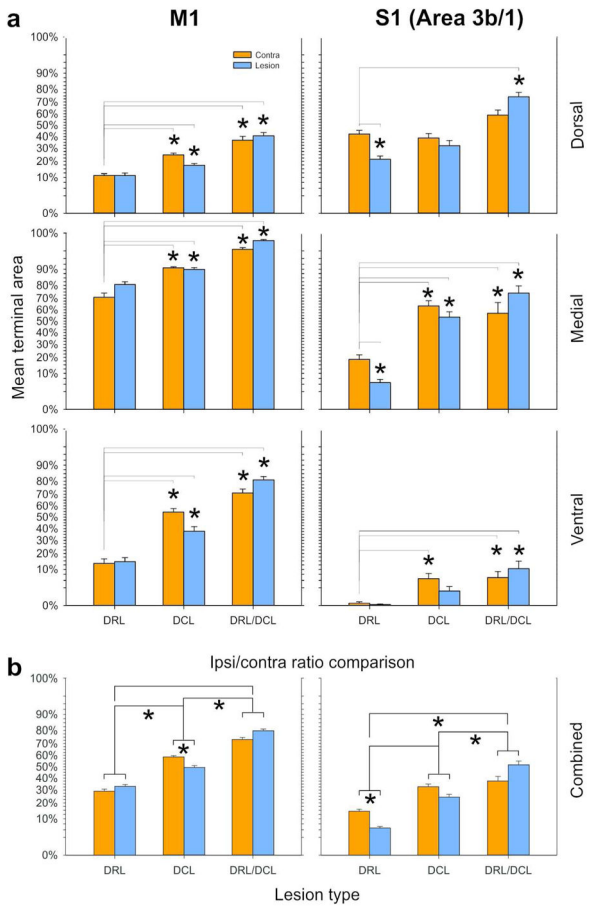

Figure 7.

Terminal bouton territory histograms for S1 and M1 CSTs. **a** Each section was divided into Dorsal, Medial, and Ventral zones, and into contralateral and ipsilateral subregions. The contralateral side in the DRL lesion group (n=2) was used as the control since this did not differ from normal control animals, or published accounts. Asterisks indicate means that differed significantly from their respective controls. Significance was defined as $P<0.0167$ (Bonferonni corrected), since we controlled for multiple comparisons. Lines are only shown where comparisons were statistically significant. Data are plotted as Repeated Measures LSM +/− SE, thus controlling for differences between monkeys and for systematic differences along the cord. Data are angular transformed (see Methods for details). **b** shows summary histograms that pooled data for dorsal, medial, and ventral subdivisions to determine differences in the sprouting response relative to the lesion. Comparisons were made between the ipsi- and contralateral sides of the spinal cord, both within and across lesion groups. Findings were always the same for monkeys within each lesion group. Asterisks indicate statistical significance. Note that following a DCL alone (n=2), more extensive terminal labeling (sprouting) was observed on the contralateral side of the cord, but this was reversed following the combined DRL/DCL (n=2).

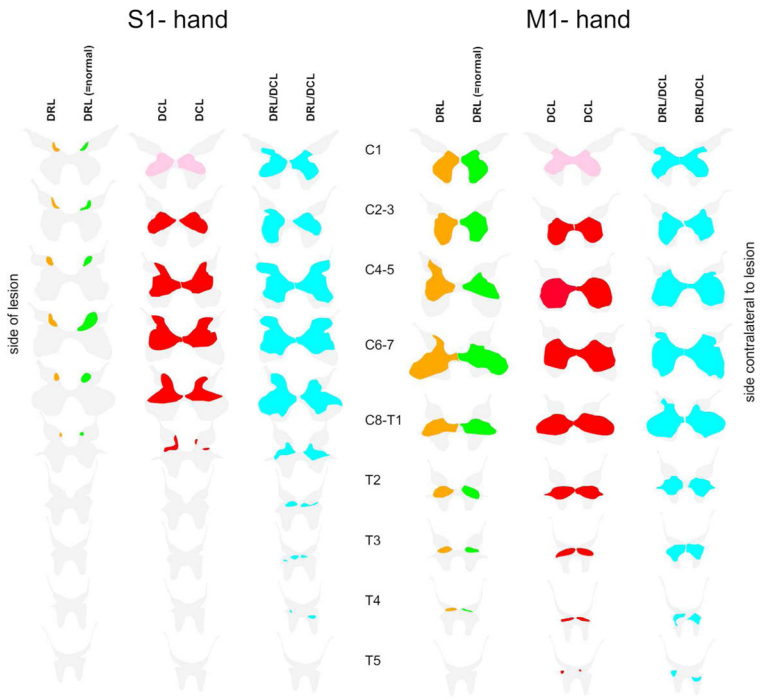

Figure 8.

Summary Schematic comparing terminal distribution patterns of CST boutons following different spinal cord lesions. Schematic combines data from monkeys and shows the averaged terminal territory for each lesion group. The green color represents normal CST terminal territory in both cases. Orange reflects the change in area following a DRL; this is reduced by ~40% for S1 and remains robust for M1 with some extension up into dorsal regions. After a DCL (red), the CST sprouts extensively on both sides of the cord for both S1 and M1. This is more pronounced when a DCL is combined with a DRL (blue); here we see hugely expanded terminal fields for both S1 and M1 which now extend further into the thoracic cord.

Table 1

Abbreviations

CST	corticospinal tract
D1–3	digits 1, 2 and 3, or thumb, index and middle fingers
DCL	dorsal column lesion
DRL	dorsal root lesion (or dorsal rhizotomy)
DRL/DCL	combined dorsal root and dorsal column lesion
M1	Primary motor cortex (Brodmann Area 4)
S1	Primary somatosensory cortex (Areas 31, 3b, 1 and 2). In this study our injections only targeted areas 3b/1

Table 2

Details of the animals whose data was used in this study.

Lesion	Monkey ID	Lesion laterality	Postoperative times		Tracer Injections	
			Time between lesion and craniotomy (wks)	Tracer transport (wks)	S1	M1
DCL	1401	Right	11	6	LYD	BDA
	1403	Right	12	6	LYD	BDA
DRL	601	Left	9.5	6	BDA	LYD
	604	Left	14	7	LYD	BDA
	602	Right	9	6	LYD	-
	603	Left	11	7	LYD	-
	701	Left	18	5	-	LYD
	1108	Left	15	7	-	LYD,BDA
2DRL/DCL	1106	Left	11	7	LYD	BDA
	1109	Left	15	7	BDA	LYD

J Comp Neurol. Author manuscript; available in PMC 2019 October 15.